2D Generalized Optical Spatial Modulation with Deep Learning-Aided Detection

Chen Chen, Lin Zeng, Xin Zhong, Shu Fu, Zhihong Zeng, Min Liu, and Harald Haas *Fellow, IEEE*

***Abstract*—In this paper, we propose a novel two-dimensional (2D) generalized optical spatial modulation (GOSM) scheme for multiple-input multiple-output optical wireless communication (MIMO-OWC) systems. By grouping two successive time slots as one time block, 2D GOSM mapping can be performed not only in the space domain but also in the time domain. Specifically, two types of 2D GOSM mapping schemes are designed, including 2D-1 and 2D-2 GOSM mappings. Moreover, to address the high complexity issue of optimal joint maximum-likelihood (ML) detection and the noise amplification and error propagation issues of zero-forcing-based ML (ZF-ML) detection, a deep neural network (DNN)-aided detection scheme is further proposed for 2D GOSM systems. Simulation results demonstrate the superiority of the proposed 2D GOSM scheme with deep learning-aided detection for high-speed and low-complexity MIMO-OWC systems.**

***Index Terms*—Optical wireless communication, multiple-input multiple-output, deep learning.**

I. Introduction

With the booming growth of mobile users in the coming years, the generated enormous data traffic will be far beyond the capacity of existing radio-frequency (RF) communication techniques. Thanks to its many inherent advantages such as abundant license-free spectrum and no electromagnetic interference radiation, optical wireless communication (OWC) has been envisioned as a promising complementary technology to alleviate the spectrum crunch [1]. In OWC systems using light-emitting diodes (LEDs) as optical transmitters, the available modulation bandwidth is usually small and hence the achievable capacity of OWC systems is greatly limited [2].

For a given modulation bandwidth, the capacity of OWC systems can be enhanced by improving the spectral efficiency of the system. So far, various techniques have been proposed to improve the spectral efficiency of bandlimited OWC systems. Particularly, by fully exploiting the spatial-domain resources, multiple-input multiple-output (MIMO) transmission has been widely shown as a promising technique for bandlimited OWC systems [3], [4]. As a digitized MIMO scheme, optical spatial modulation (OSM) has attracted great interest recently, owing to its negligible inter-channel interference, high power efficiency and low transceiver complexity [5], [6]. Nevertheless, it is very challenging for OSM systems to achieve a high spectral efficiency. In order to enhance the spectral efficiency of OSM, generalized OSM (GOSM) schemes have been further proposed, which activate more than one LED to transmit the same constellation symbol at each time slot [7], [8]. Besides spectral efficiency enhancement, GOSM can also provide substantial spatial diversity to increase the signal-to-noise ratio (SNR) of the received constellation symbols. However, in all the existing GOSM systems, the GOSM mapping is one-dimensional (1D) which is generally performed in the spatial domain only.

In this paper, we for the first time propose and investigate a novel two-dimensional (2D) GOSM scheme for bandlimited MIMO-OWC systems. By grouping two successive time slots as one time block, GOSM mapping can be performed in both the spatial domain and the time domain. More specifically, two types of 2D GOSM mapping schemes, i.e., 2D-1 and 2D-2 GOSM mappings, are designed within one time block. Moreover, three detection schemes, including joint maximum-likelihood (ML) detection, zero-forcing-based ML (ZF-ML) detection and deep neural network (DNN)-aided detection, are further proposed. It has been shown that the DNN-aided detection is able to mitigate the adverse effects of both noise amplification and error propagation suffered by the ZF-ML detection, while achieving near optimal performance as the joint ML detection with low computational complexity [8], [9]. Numerical simulations are conducted to evaluate and compare the performance of the conventional 1D GOSM and the proposed 2D GOSM with different detection schemes.

II. System Model

A typical MIMO-OWC system is considered here, which is equipped with N_t LEDs and N_r photo-detectors (PDs). Letting $\mathbf{s} = [s_1, s_2, \cdots, s_{N_t}]^T$ represent the transmitted signal vector, $\mathbf{H}$ denote the $N_r \times N_t$ MIMO channel matrix and $\mathbf{n} = [n_1, n_2, \cdots, n_{N_r}]^T$ be the additive noise vector, the received signal vector $\mathbf{y} = [y_1, y_2, \cdots, y_{N_r}]^T$ can be given by

$$\mathbf{y} = \mathbf{H}\mathbf{s} + \mathbf{n}, \tag{1}$$

where the MIMO channel matrix $\mathbf{H}$ can be expressed by

$$\mathbf{H} = \begin{bmatrix} h_{11} & \cdots & h_{1N_t} \\ \vdots & \ddots & \vdots \\ h_{N_r1} & \cdots & h_{N_rN_t} \end{bmatrix}, \tag{2}$$

This work was supported in part by the National Natural Science Foundation of China under Grant 61901065 and in part by the Natural Science Foundation of Chongqing under Grant cstc2021jcyj-msxmX0480.

C. Chen, L. Zeng, X. Zhong, S. Fu, and M. Liu are with the School of Microelectronics and Communication Engineering, Chongqing University, Chongqing 400044, China (e-mail: {c.chen, 202012021008, 201912131098, shufu, liumin}@cqu.edu.cn).

Z. Zeng is with the LiFi Research and Development Centre, Institute for Digital Communications, The University of Edinburgh, EH9 3JL, UK (e-mail: zhihong.zeng@ed.ac.uk).

H. Haas is with the Technology Innovation Centre, Department of Electronic and Electrical Engineering, University of Strathclyde, Glasgow G1 1RD, U.K. (e-mail: harald.haas@strath.ac.uk).

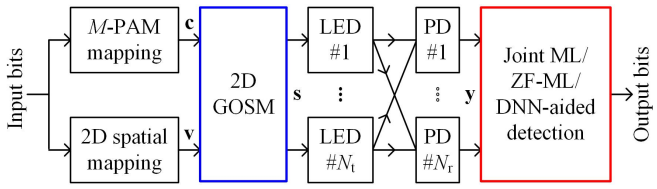

Fig. 1. Schematic diagram of the proposed 2D GOSM system.

where h_{rt} denotes the direct current (DC) channel gain between the t-th LED and the r-th PD with $r = 1, 2, \cdots, N_r$ and $t = 1, 2, \cdots, N_t$. Without loss of generality, we assume that each LED follows the Lambertian radiation pattern and only the line-of-sight (LOS) transmission is considered. It is generally reasonable to neglect the non-LOS component since the non-LOS component usually has much lower electrical power than that of the LOS component during most channel conditions [3]. Thus, h_{rt} can be calculated by

$$h_{rt} = \frac{(l+1)\rho A}{2\pi d_{rt}^2}\cos^l(\varphi_{rt})T_s(\theta_{rt})g(\theta_{rt})\cos(\theta_{rt}), \quad (3)$$

where $l = -\ln 2/\ln(\cos(\Psi))$ represents the Lambertian emission order and Ψ is the semi-angle at half power of the LED; ρ and A denote the responsivity and the active area of the PD, respectively; the distance, the angle of emission and the angle of incidence between the t-th LED and the r-th PD are expressed by d_{rt}, φ_{rt} and θ_{rt}, respectively; $T_s(\theta_{rt})$ is the gain of optical filter; $g(\theta_{rt}) = \frac{n^2}{\sin^2\Phi}$ is the gain of optical lens, where n and Φ denote the refractive index and the half-angle field-of view (FOV) of the optical lens, respectively.

In typical MIMO-OWC systems, the additive noise consists of shot noise, thermal noise and possibly excess noise, which can be generally modeled as a real-valued additive white Gaussian noise (AWGN) with zero mean and power $P_n = N_0 B$, where N_0 and B indicate the noise power spectral density (PSD) and the signal bandwidth, respectively.

III. 2D GOSM FOR OWC

In this section, we first introduce the principle of 2D GOSM and then three spatial mapping schemes are described. Finally, three detection schemes for 2D GOSM are described.

A. Principle of 2D GOSM

Fig. 1 illustrates the schematic diagram of the proposed 2D GOSM system, where M-ary pulse amplitude modulation (M-PAM) is adopted. For M-PAM modulation, the intensity levels can be expressed as $I_m = \frac{2Im}{M+1}$ $(m = 1, \cdots, M)$. It can be seen that the input bits are first divided into two parts, i.e., the constellation part and the spatial part, which are then mapped into a PAM symbol vector $\mathbf{c}$ and a spatial index vector $\mathbf{v}$, respectively. Subsequently, 2D GOSM mapping is executed to generate the transmitted signal vector $\mathbf{s}$. At the receiver side, 2D GOSM detection, including the joint ML detection, the ZF-ML detection and the DNN-aided detection, is performed to yield the final output bits.

B. Three Spatial Mapping Schemes

In this subsection, three spatial mapping schemes are introduced, including conventional 1D spatial mapping and two novel 2D spatial mapping schemes, i.e., 2D-1 spatial mapping and 2D-2 spatial mapping.

1) 1D Spatial Mapping: Fig. 2(a) shows the principle of conventional 1D spatial mapping, where N out of N_t LEDs are activated to transmit the same M-PAM symbol at each time slot, taking $N_t = 4$ and $N = 2$ for example. As a result, there are $C(N_t, N)$ possible LED activation patterns and $\lfloor \log_2 C(N_t, N) \rfloor$ spatial bits can be transmitted, where $C(\cdot,\cdot)$ denotes the binomial coefficient and $\lfloor \cdot \rfloor$ represents the floor operation. Hence, the spectral efficiency (bits/s/Hz) of 1D GOSM systems using M-PAM modulation is given by

$$R_{\text{1D}} = \log_2 M + \lfloor \log_2 C(N_t, N) \rfloor. \quad (4)$$

2) 2D-1 Spatial Mapping: Fig. 2(b) depicts the principle of 2D-1 spatial mapping, where two successive time slots are grouped as one time block. Specifically, for each time slot within a given time block, N out of N_t LEDs are activated to transmit the same M-PAM symbol and 2D-1 spatial mapping is executed over two successive time slots within each time block. Taking the first time block τ_1 as an example, there are $C(N_t, N)$ possible LED activation patterns for both time slots t_1 and t_2. Hence, the total number of possible LED activation patterns over two time slots t_1 and t_2 within the time block τ_1 is given by $(C(N_t, N))^2$. Moreover, two different M-PAM symbols can be transmitted in the two time slots within one time block. Therefore, assuming M_1-PAM and M_2-PAM are respectively adopted in the first and the second time slots within each time block, the spectral efficiency (bits/s/Hz) of 2D-1 GOSM systems is obtained by

$$R_{\text{2D-1}} = \frac{1}{2}\log_2(M_1 M_2) + \frac{1}{2}\lfloor 2\log_2 C(N_t, N) \rfloor. \quad (5)$$

3) 2D-2 Spatial Mapping: The principle of 2D-2 spatial mapping is shown in Fig. 2(c). Similarly, two successive time slots are grouped as one time block and two different M-PAM symbols, i.e., M_1-PAM and M_2-PAM, are transmitted in the first and the second time slots within each time block, respectively. Differing from 2D-1 spatial mapping where N out of N_t LEDs are activated to transmit signal at each time slot, the number of activated LEDs in each time slot is not fixed in 2D-2 spatial mapping and only the total number of activated LEDs within each time block is fixed. Specifically, for each time block, $2N$ out of totally $2N_t$ LEDs are activated to transmit signals and the number of activated LEDs at two time slots within the time block can be different. Thus, for 2D-2 spatial mapping, there are totally $C(2N_t, 2N)$ possible LED activation patterns within one time block. Note that there should be at least one activated LED to transmit signal at each time slot within the time block, to ensure the successful transmission of constellation symbols. Consequently, the spectral efficiency (bits/s/Hz) of 2D-2 GOSM systems is given by

$$R_{\text{2D-2}} = \frac{1}{2}\log_2(M_1 M_2) + \frac{1}{2}\lfloor \log_2 C(2N_t, 2N) \rfloor. \quad (6)$$

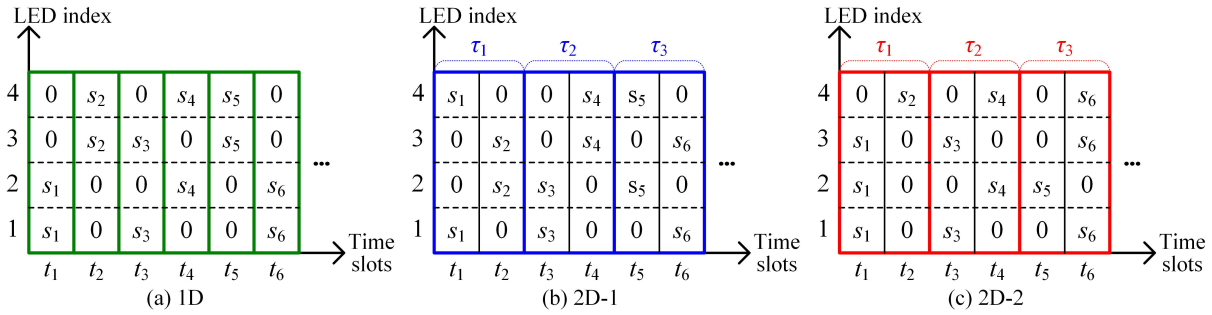

Fig. 2. Principle of (a) 1D GOSM, (b) 2D-1 GOSM and (c) 2D-2 GOSM, where N_t = 4 and N = 2.

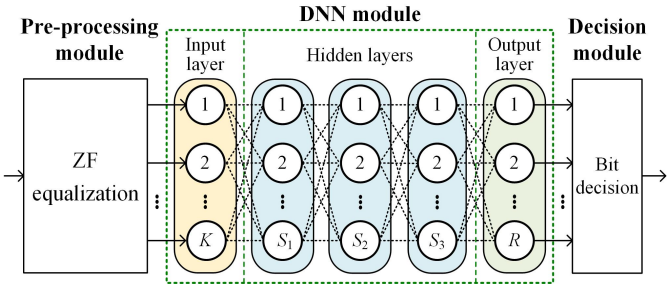

Fig. 3. Schematic diagram of the DNN-aided detection.

C. Three Detection Schemes for 2D GOSM

1) Joint ML Detection: Assuming perfect knowledge of the channel, joint ML detection is the optimal detection scheme for 2D GOSM systems using M-PAM modulation. Under joint ML detection, the transmitted signal vector $\mathbf{s}$ is estimated by

$$\hat{\mathbf{s}} = \arg\min_{\mathbf{s}} ||\mathbf{y} - \mathbf{H}\mathbf{s}||^2, \tag{7}$$

where $\|\cdot\|$ denotes the Euclidean norm. Although joint ML detection can achieve optimal performance, its computational complexity is relatively high and hence it might not be feasible in practical applications.

2) ZF-ML Detection: In comparison to the joint ML detection, ZF-ML detection achieves sub-optimal performance with much reduced computational complexity [9]. To apply ZF-ML detection in 2D GOSM systems, ZF equalization is first performed on the received signal vector $\mathbf{y}$ and thus the estimate of the transmitted signal vector $\mathbf{s}$ is expressed by

$$\hat{\mathbf{s}}_{\text{ZF}} = \mathbf{H}^{\dagger}\mathbf{y} = \mathbf{s} + \mathbf{H}^{\dagger}\mathbf{n}, \tag{8}$$

where $\mathbf{H}^{\dagger} = (\mathbf{H}^{*}\mathbf{H})^{-1}\mathbf{H}^{*}$ denotes the pseudo inverse of $\mathbf{H}$. After that, both the spatial index vector and the constellation symbol vector can be obtained from $\hat{\mathbf{s}}_{\text{ZF}}$ via ML detection. Despite its low computational complexity, ZF-ML detection suffers from the adverse effects of both noise amplification and error propagation [4], [10].

3) DNN-Aided Detection: In order to simultaneously address the high complexity issue of joint ML detection and the noise amplification and error propagation issues of ZF-ML detection, a DNN-aided detection scheme is proposed for 2D GOSM systems. Fig. 3 depicts the schematic diagram of the DNN-aided detection scheme, which mainly consists of a pre-processing module, a DNN module and a decision module. The pre-processing module is used to perform ZF equalization on the received signal vector $\mathbf{y}$ so as to get the input vector of the DNN module. The DNN module contains one input layer, three hidden layers and one output layer. For the 2D GOSM systems with N_t LEDs, the input vector contains all the $2N_t$ symbols within one time block and hence the input layer contains $K = 2N_t$ neurons. Moreover, three fully connected hidden layers are used to learn the statistical characteristics of both the input signal and the additive noise. Note that the number of hidden layers and the number of neurons adopted in each hidden layer are obtained after multiple trials, which can ensure that the DNN achieves satisfactory performance. The number of neurons in the l-th $(1 \leqslant l \leqslant 3)$ hidden layer is denoted by S_l and the rectified linear unit (ReLU) function, i.e., $f_{\text{ReLU}}(\alpha) = \max(0, \alpha)$, is used as the activation function. For the output layer, it consists of R neurons, which is corresponding to the number of bits that can be transmitted during one time block, and the Sigmoid function, i.e., $f_{\text{Sigmoid}}(\alpha) = 1/(1 + \exp^{-\alpha})$, is adopted as the activation function to map the output into the interval (0,1).

In addition, the decision module is utilized to generate the final binary bits. Letting $\mathbf{z}_5 = [z_1, z_2, \cdots, z_R]^T$ be the input of the decision module, the estimated bit information $\hat{u}_q$ $(1 \leqslant q \leqslant R)$ can be obtained by

$$\hat{u}_q = \begin{cases} 0, & z_q < 0.5, \\ 1, & z_q \geq 0.5. \end{cases} \tag{9}$$

Finally, we exploit the mean-squared error (MSE) loss function to measure the difference between the transmitted bit vector $\mathbf{u}$ and the estimated bit vector $\hat{\mathbf{u}}$, which is denoted by

$$e_{\text{MSE}} = \frac{1}{R}\| \hat{\mathbf{u}} - \mathbf{u} \|^2. \tag{10}$$

IV. Simulation Results

In this section, simulations are performed to evaluate the performance of the proposed 2D GOSM systems using different detection schemes with different spectral efficiencies. In our simulations, we consider a 4×4 MIMO-OWC system in

TABLE I
SIMULATION PARAMETERS

Parameter	Value
Room dimension	4 m × 4 m × 3 m
LED spacing	2 m
APD spacing	15 cm
Semi-angle at half power of LED	65°
Gain of optical filter	0.9
Refractive index of optical lens	1.5
Half-angle FOV of optical lens	65°
Responsivity of APD	15 A/W
Height of receiving plane	1 m
Active area of APD	19.6 mm^2
Noise PSD	$10^{-22}A^2$/Hz
Modulation bandwidth	20 MHz
Number of LEDs	4
Number of activated LEDs	2
Number of APDs	4
Receiver location	(1.5 m, 1.5 m, 1 m)

TABLE II
PARAMETERS OF DNN-AIDED DETECTORS

	Parameter	4 bits/s/Hz	5 bits/s/Hz
1D	number of training set	200000	600000
	number of neurons	20-24-20	120-128-120
	mini-batch size	100	200
2D-1	number of training set	300000	400000
	number of neurons	34-40-34	74-80-74
	mini-batch size	100	100
2D-2	number of training set	400000	500000
	number of neurons	60-64-60	120-128-120
	mini-batch size	200	200

TABLE III
PAM ORDER OF DIFFERENT SCHEMES

Scheme	4 bits/s/Hz	5 bits/s/Hz
1D	$M = 4$	$M = 8$
2D-1	$M_1 = 2$, $M_2 = 4$	$M_1 = 4$, $M_2 = 8$
2D-2	$M_1 = 2$, $M_2 = 2$	$M_1 = 4$, $M_2 = 4$

a typical 4 m × 4 m × 3 m room. The 2 × 2 LED array is mounted at the center of the ceiling and the height of the receiving plane is 1 m. The key simulation parameters are listed in Table I. In order to accelerate the convergence speed, the mini-batch technique is employed in the training phase and the learning rate is 0.01. Moreover, the validation set includes 5×10^4 randomly generated symbol vectors and Adamax is used as optimizer. The parameters of the DNN-aided detectors for 1D, 2D-1 and 2D-2 GOSM systems are summarized in Table II. According to (4), (5) and (6), the required PAM orders of 1D, 2D-1 and 2D-2 GOSM systems to achieve target spectral efficiencies of 4 and 5 bits/s/Hz are given in Table III. Moreover, we evaluate the bit error rate (BER) performance with respect to the transmitted SNR in the simulations and the reason can be found in [4].

A. MSE Loss

We first analyze the MSE loss of the proposed DNN-aided detector and the results are given in Fig. 4. As we can see, the MSE decreases rapidly with the increased number of epochs

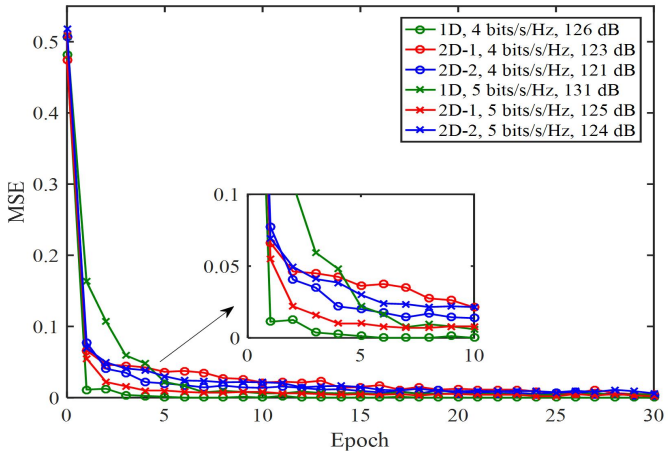

Fig. 4. MSE loss vs. epoch for the proposed DNN-aided detector.

for 1D, 2D-1 and 2D-2 GOSM systems with different spectral efficiencies and training SNRs. Here, training SNR represents the transmitted SNR selected to train the DNN. Moreover, for a higher spectral efficiency, a larger training SNR is required to successfully train the DNN. It can be clearly observed that only about 30 epochs are needed to make the MSE loss converge for all cases. Hence, the proposed DNN-aided detector can be deployed rapidly in practical applications.

B. BER Performance

We further evaluate and compare the BER performance of 1D, 2D-1 and 2D-2 GOSM systems with different detection schemes and spectral efficiencies. Figs. 5(a) and (b) compare the BER versus transmitted SNR with spectral efficiencies of 4 and 5 bits/s/Hz, respectively. For a spectral efficiency of 4 bits/s/Hz as shown in Fig. 5(a), when using ZF-ML detection, 2D-1 GOSM performs slightly better than 1D GOSM while 2D-2 GOSM outperforms 2D-1 GOSM by an SNR gain of 2.2 dB. In contrast, when the DNN-aided detection with optimal training SNRs is applied, all the three GOSM systems obtain nearly the same BER performance as that applying joint ML detection. More specifically, the required SNRs to reach BER = 10^{-3} are 126, 125.4 and 123.4 dB for 1D, 2D-1 and 2D-2 GOSM systems, respectively. Hence, a remarkable SNR gain of 26 dB is achieved for all three GOSM systems compared with that using the ZF-ML detection, which is mainly because that the DNN-aided detection is able to eliminate noise amplification. Similarly, 1D and 2D-1 GOSM obtains comparable BER performance, while 2D-2 GOSM obtains an SNR gain of 2.6 dB in comparison to 2D-1 GOSM at BER = 10^{-3}. For a higher spectral efficiency of 5 bits/s/Hz as shown in Fig. 5(b), 2D-1 GOSM still slightly outperforms 1D GOSM when adopting ZF-ML detection. However, 2D-1 GOSM achieves an SNR gain of 1.7 dB over 1D GOSM when applying DNN-aided detection, which suggests that the DNN-aided detection is able to mitigate error propagation. In addition, an SNR gain of 1.7 dB is also achieved by 2D-2 GOSM in comparison to 2D-1 GOSM. It can be clearly observed from Figs. 5(a) and (b) that 2D-2 GOSM with DNN-aided detection achieves the best BER performance among all the considered schemes.

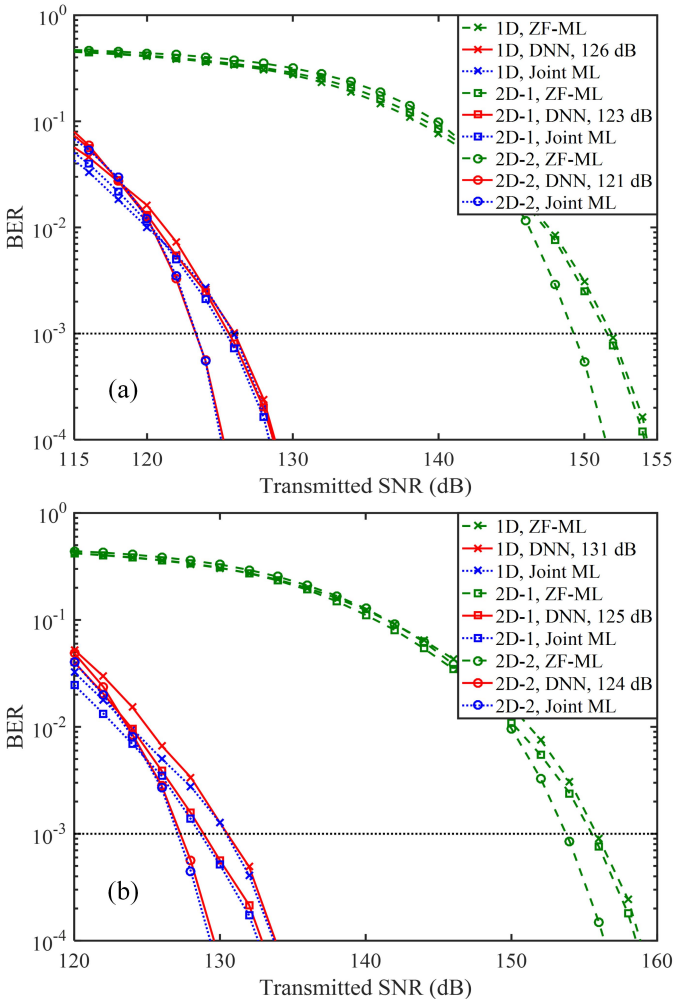

Fig. 5. BER vs. transmitted SNR for 1D, 2D-1 and 2D-2 GOSM systems with a spectral efficiency of (a) 4 bits/s/Hz and (b) 5 bits/s/Hz.

C. Computational Complexity

Finally, we compare the computational complexity of three detection schemes in terms of computation time. The simulation was performed using JetBrains PyCharm with an AMD Ryzen 5 3600 CPU, 16 GB RAM, and NVIDIA GeForce GTX 1660 SUPER GPU. Considering the fact that once the DNN-aided detector has been trained, it can be used for signal detection for a long time without further retraining, unless the system parameters have been changed. Therefore, only the complexity in the online detecting phase needs to be considered, while the complexity of the offline training process is not taken into consideration [8], [9]. Table IV compares the computation time of three detection schemes with two spectral efficiencies of 4 and 5 bits/s/Hz. For the 1D GOSM system with a spectral efficiency of 4 bits/s/Hz, the computation time of the DNN-aided detector is comparable as that of the ZF-ML detector, which is much shorter than that of the joint ML detector. For the 2D-1 and 2D-2 GOSM systems with a spectral efficiency of 4 bits/s/Hz, the computation time of the DNN-aided detector becomes shorter than that of the ZF-ML detector. The same conclusion can also be found for 1D, 2D-1 and 2D-2 GOSM systems with a spectral efficiency of 5 bits/s/Hz. Therefore, the proposed DNN-aided detector is shown to be a low-complexity detector that can achieve near optimal BER performance.

TABLE IV
COMPARISON OF COMPUTATION TIME

Scheme		4 bits/s/Hz	5 bits/s/Hz
1D	Joint ML	4.61 s	7.31 s
	ZF-ML	1.31 s	1.51 s
	DNN	1.25 s	1.50 s
2D-1	Joint ML	4.03 s	6.13 s
	ZF-ML	1.77 s	1.95 s
	DNN	1.39 s	1.66 s
2D-2	Joint ML	7.04 s	10.51 s
	ZF-ML	2.78 s	2.94 s
	DNN	1.63 s	1.81 s

V. CONCLUSION

In this paper, we have proposed a novel 2D GOSM scheme with deep learning-aided detection for MIMO-OWC systems. Compared with conventional 1D GOSM mapping, the proposed two 2D GOSM mapping schemes, namely 2D-1 and 2D-2 GOSM mappings, can achieve higher spectral efficiencies. Moreover, the proposed DNN-aided detection obtains comparable BER performance as the optimal joint ML detection, but with much reduced computational complexity. Our simulation results show that 2D-2 GOSM with DNN-aided detection achieves the best BER performance for two target spectral efficiencies. Therefore, the proposed deep learning-aided 2D GOSM scheme can be a promising candidate for high-speed and low-complexity MIMO-OWC systems.

REFERENCES

[1] T. Cogalan and H. Haas, "Why would 5G need optical wireless communications?" in *Proc. IEEE Ann. Int. Symp. Pers., Indoor Mobile Radio Commun. (PIMRC)*, Oct. 2017, pp. 1–6.
[2] S. Rajagopal, R. D. Roberts, and S.-K. Lim, "IEEE 802.15. 7 visible light communication: modulation schemes and dimming support," *IEEE Commun. Mag.*, vol. 50, no. 3, Mar. 2012.
[3] T. Fath and H. Haas, "Performance comparison of MIMO techniques for optical wireless communications in indoor environments," *IEEE Trans. Commun.*, vol. 61, no. 2, pp. 733–742, Feb. 2013.
[4] C. Chen, X. Zhong, S. Fu, X. Jian, M. Liu, H. Yang, A. Alphones, and H. Y. Fu, "OFDM-based generalized optical MIMO," *J. Lightw. Technol.*, vol. 39, no. 19, pp. 6063–6075, Oct. 2021.
[5] R. Mesleh, H. Elgala, and H. Haas, "Optical spatial modulation," *J. Opt. Commun. Netw.*, vol. 3, no. 3, pp. 234–244, Mar. 2011.
[6] M. D. Soltani, M. A. Arfaoui, I. Tavakkolnia, A. Ghrayeb, M. Safari, C. M. Assi, M. O. Hasna, and H. Haas, "Bidirectional optical spatial modulation for mobile users: Toward a practical design for LiFi systems," *IEEE J. Sel. Areas Commun.*, vol. 37, no. 9, pp. 2069–2086, Sep. 2019.
[7] C. R. Kumar and R. Jeyachitra, "Power efficient generalized spatial modulation MIMO for indoor visible light communications," *IEEE Photon. Technol. Lett.*, vol. 29, no. 11, pp. 921–924, Jun. 2017.
[8] C. Chen, L. Zeng, X. Zhong, S. Fu, M. Liu, and P. Du, "Deep learning-aided OFDM-based generalized optical quadrature spatial modulation," *IEEE Photon. J.*, vol. 14, no. 1, p. 7302306, Feb. 2022.
[9] T. Wang, F. Yang, and J. Song, "Deep learning-based detection scheme for visible light communication with generalized spatial modulation," *Opt. Exp.*, vol. 28, no. 14, pp. 21 202–21 209, Sep. 2020.
[10] C. Chen, H. Yang, P. Du, W.-D. Zhong, A. Alphones, Y. Yang, and X. Deng, "User-centric MIMO techniques for indoor visible light communication systems," *IEEE Syst. J.*, vol. 14, no. 3, pp. 3202–3213, Sep. 2020.